Mon. Not. R. Astron. Soc. **000**, 000–000 (0000) Printed 9 November 1998 (MN LATEX style file v1.4)

Circumstellar Kinematics and the Measurement of Stellar Mass for the Protostars TMC1 and TMC1A

David W. Brown and Claire J. Chandler
Mullard Radio Astronomy Observatory, Cavendish Laboratory, Madingley Road, Cambridge, CB3 0HE

9 November 1998

ABSTRACT
We present observations of two protostars in the Taurus Molecular Cloud, TMC1 and TMC1A, obtained using the Owens Valley mm array. ^{13}CO and C^{18}O J=1–0 data, and observations at 2.7mm in the continuum, reveal the presence of molecular gas in circumstellar envelopes out to a radius of 1000 AU. The velocity field in these envelopes is well described by Keplerian rotation and shows no signature of infall motions. The dynamical masses of the central objects, derived from the velocity structure of the isotopic CO emission, are 0.2–0.4 $M_\odot$ for TMC1, and 0.35–0.7 $M_\odot$ for TMC1A depending upon the assumed inclination, with typical uncertainties in the mass measurements at a given inclination of 10%. Our determinations of the stellar masses enable us to place upper limits on the accretion rates in these sources of $\dot{M} \lesssim 4 \times 10^{-7}$ $M_\odot$ yr^{-1}, which is at least an order of magnitude lower than that needed to assemble the observed mass with a constant $\dot{M}$ assuming a typical age of 10^5 yr. We conclude that the accretion rate is not constant in time.

Key words: Stars: formation – stars: circumstellar matter – stars: individual alphanumeric: IRAS 04381+2540 – stars: individual alphanumeric: IRAS 04365+2535 – ISM: kinematics and dynamics

1 INTRODUCTION

It remains the case that the most common model used for interpreting observations of low-mass star formation is that of the collapse of a singular isothermal sphere as originally formulated by Shu (1977), and its subsequent adaption by Terebey, Shu, & Cassen (1984) to include the effects of slow rotation. In this model material approaches a $\rho \propto r^{-2}$ density distribution quasi-statically, which being highly unstable to perturbations, collapses to form a hydrostatic core on a free-fall time-scale. This results in an infall region with $\rho \propto r^{-1.5}$ that expands outwards at the isothermal sound speed, a. A consequence of this inside-out collapse is that it predicts a mass accretion rate of $\dot{M} \sim a^3/G$ which is constant in time. For cloud core temperatures of ~ 10 K typical of the Taurus Molecular Cloud the Shu model predicts mass accretion rates of $\dot{M} \sim 10^{-5}$ $M_\odot$ yr^{-1}. To build up a stellar mass of ~ 1 $M_\odot$ would therefore require the lifetime of the collapse phase to be $\sim 10^5$ yr, in agreement with lifetimes of embedded protostars derived from source counts (Kenyon et al. 1990).

For a protostar of mass M_* and radius R_* the accretion luminosity, $L_{\rm acc}$, is given by

$$L_{\rm acc} = GM_*\dot{M}(t)/R_*. \quad (1)$$

Assuming a typical stellar mass of Class 0/I protostars in Taurus of ~ 0.5 $M_\odot$, and a radius R_* of 3 $R_\odot$ (Stahler 1988), the observed luminosity of the embedded protostars in Taurus implies an accretion rate onto the star lower than that predicted by the Shu model, by at least an order of magnitude. This discrepancy has been termed the "luminosity problem" by Kenyon et al. (1990), and it implies that the Shu picture of cloud collapse with a constant $\dot{M}$ cannot fully explain star formation as we observe it in Taurus. An alternative is to have a mass accretion rate that changes with time. For example, in the hydrodynamical calculations carried out by Foster & Chevalier (1993) an isothermal sphere with uniform density distributions in the centre collapses from a marginally stable equilibrium condition, and the infall rate steadily declines after an initial high accretion rate during stellar core formation. Alternatively, a time-dependent accretion mechanism similar to that proposed for FU Orionis type outbursts in pre-main sequence stars may be appropriate, where the protostar spends most of its time in a low accretion rate state and builds up its mass mainly through periodic phases of high accretion through a disc (Kenyon et al. 1990).

Although the unknown accretion history makes determination of the age of an embedded protostar highly uncertain, a firm observational constraint on these alternative accretion histories could be provided if values of $\dot{M}$ as a function of M_* could be established. Since accreting protostars are, by definition, surrounded by circumstellar material, the central star is heavily obscured and often undetected even in the infrared, so the stellar mass must be measured by more indirect means. The only reliable way of measuring M_* for embedded sources is therefore through the kinematics of the circumstellar material. Observations of typical angular momenta of star forming cores (Goodman et al. 1993) suggest that it is unlikely that cloud cores can undergo spherical collapse. Thus for infalling material the low angular momentum gas can be accreted while

© 0000 RAS

the high angular momentum gas rotates about the central star. The large scale velocity gradients can therefore be used to determine M_*. Once M_* is established, limits on $\dot{M}$ can be derived from equation 1.

This paper uses interferometric observations of the J=1–0 lines of ^{13}CO and C^{18}O, as well as 2.7mm continuum emission, to investigate the circumstellar environments and kinematics of the molecular gas surrounding two embedded protostars in Taurus, IRAS 04381+2540 (hereafter TMC1), and IRAS 04365+2535 (hereafter TMC1A). Both sources have been classified as Class I protostars, with ages less than 10^5 years (e.g., Chandler, Barsony, & Moore 1998), and their low bolometric temperatures, 139K for TMC1 and 172K for TMC1A (Chen et al. 1995), make them among the cooler protostars in the Taurus star forming complex. The observations of their circumstellar envelopes reveal rotational motion in both sources, allowing us to place stringent limits on the masses of the central protostars and on the current accretion rate.

2 OBSERVATIONS

Observations of the 2.7mm continuum, the ^{13}CO (1–0) line at 110.2 GHz, and the C^{18}O (1–0) line at 109.8 GHz were made towards TMC1 and TMC1A using the Owens Valley Millimeter Array in 1992 April and May. Three 10.4m dishes were used in configurations with baselines up to 55m E–W, and 80m N–S. The CO lines were placed in the lower sideband resulting in single sideband system temperatures of ∼300–500 K. Corrections for changes in phase and amplitude due to instrumental drifts were made by switching between the sources and the quasar 0420−014, and the absolute flux density calibration was determined from measurements of 3C454.3 and 3C273. The uncertainty in the flux density scale is estimated to be approximately 10%.

Spectral line data were obtained using a digital correlator with 4 modules, 2 dedicated to each CO line, resulting in 60 Hanning smoothed channels per line, with a resolution of 0.063 MHz (0.17 km s^{-1}). Continuum measurements were made simultaneously in a 350 MHz broad-band channel. Data were calibrated using software specific to the OVRO mm array (Scoville et al. 1993), and imaged using the AIPS software package. Maps were made with a weighting intermediate between natural and uniform weighting ('robust' weighting: Briggs 1995), resulting in synthesised beams of $11'' \times 7''$ (FWHM) at P.A.=−3°. The rms noise in the final images is approximately 0.2 Jy beam^{-1} in the 0.17 km s^{-1} spectral line channels, and 2.6 mJy beam^{-1} in the continuum images.

3 RESULTS

3.1 2.7mm Continuum

Continuum emission at 2.7mm is detected for both TMC1 and TMC1A, with peak flux densities and statistical uncertainties of 11.9±2.6 mJy beam^{-1} and 46.1±2.6 mJy beam^{-1} respectively. Images of the continuum emission are displayed in Fig. 1. The peak positions are located at α_{1950}=04^{h}38^{m}08.66^s, δ_{1950}=25°40′50.9″ for TMC1, and α_{1950}=04^{h}36^{m}31.37^s, δ_{1950}=25°35′54.4″ for TMC1A, with uncertainties of approximately 1.0″ and 0.4″ respectively. These positions are in good agreement with independent interferometric measurements of these sources (Terebey, Chandler & André 1993; Hogerheijde et al. 1997) and are taken to be the positions

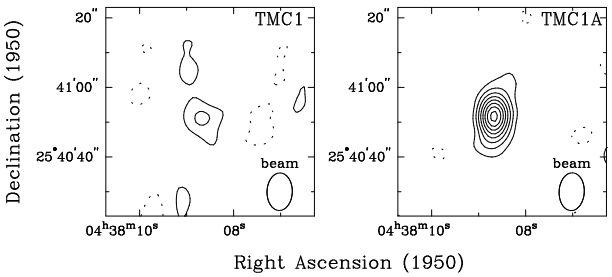

Figure 1. The 2.7mm continuum emission from TMC1 (left) and TMC1A (right). Contour levels for both maps are at 2σ intervals of 5.2 mJy beam^{-1}.

of the central stars. The continuum emission is unresolved in both cases.

Compact millimetre continuum emission from embedded protostars is usually interpreted as arising from warm dust in a circumstellar disc (e.g., Beckwith et al. 1990; Ohashi et al. 1996). Such discs have now been imaged in nearby star forming regions with sub-arcsecond resolution, and have typical radii of 60–80 AU, e.g., HL Tau (Lay et al. 1994, Lay, Carlstrom, & Hills 1997; Wilner et al. 1996), T Tau (van Langevelde, Van Dishoeck, & Blake 1994) and L1551 (Looney, Mundy, & Welch. 1997). The high optical depths in compact discs also lead to a flatter spectrum at wavelengths longer than 1mm than would be expected from the envelope, appearing as an excess of emission (Terebey et al. 1993). Surveys at 2.7mm have shown that a compact dust disc is required to account for the observed fluxes towards a sizeable fraction of embedded protostars; in particular, the recent work by Hogerheijde et al. (1997), which included TMC1 and TMC1A, revealed discs in ∼ 50% of embedded protostellar systems in Taurus. Of the two protostars presented here it appears that TMC1A contains an unresolved dust disc, with a maximum radius of the order 100–200 AU given that it was unresolved in a 3″ beam (Hogerheijde et al. 1997). Hogerheijde et al. find no variation of flux with uv-distance, and their reported flux in a 3″ beam is also similar to that detected, at lower resolution, in our observations. It is not clear if there is an unresolved component to the TMC1 emission. Although the flux is higher in our beam relative to the 3″ beam of Hogerheijde et al., consistent with extended emission, there is low signal to noise in both datasets, and the evidence for a disc from the continuum data is inconclusive.

The continuum emission can be used to derive the mass of circumstellar material in these sources, assuming that it is optically thin. Adopting a dust temperature T_d one can derive the circumstellar mass from the total flux density using $M_{circ} = F_\nu D^2 / \kappa_\nu B_\nu(T_d)$ (Hildebrand 1983), where F_ν is the flux density, κ_ν is the frequency-dependent dust opacity, B_ν is the Planck function at dust temperature T_d, and D the distance to the source. We adopt the same expression as Beckwith & Sargent (1991) for the dust opacity, $\kappa_\nu = 0.01(\nu/10^{12}\,\mathrm{Hz})^\beta\ \mathrm{m^2 kg^{-1}}$, and assuming the Rayleigh–Jeans approximation holds we obtain,

$$M_{circ} \sim 1.5 \times 10^{-6} \left[\frac{F_\nu}{\mathrm{Jy}}\right] \left[\frac{D}{\mathrm{pc}}\right]^2 \times \left[\frac{T_d}{\mathrm{K}}\right]^{-1} \left[\frac{\nu}{(10^{12}\,\mathrm{Hz})}\right]^{-(2+\beta)} \mathrm{M}_\odot \,. \quad (2)$$

The power law dependence of the dust mass opacity coefficient, β, is dependent on the dust properties. A value of β ∼ 2 is commonly adopted for the general interstellar medium (cf. Draine &

Lee 1984), but calculations show that changes in the composition, shape and growth of dust grains can all act to lower β (e.g., Wright 1987, Krügel & Siebenmorgen 1994, Pollack et al. 1994). These predictions are consistent with measurements of T Tauri stars which require values for $\beta \sim 1$ to fit the observations (Beckwith & Sargent 1991; Mannings & Emerson 1994).

Fitting a power law dependence on frequency, $F_\nu \propto \nu^\alpha$, through the flux measurements of TMC1A from Hogerheijde et al. (1997) at 2.7mm and 3.4mm we find $F_\nu \propto \nu^{2.6\pm0.8}$ for the compact dust component. If optically thin emission is assumed, and the Rayleigh-Jeans approximation holds, then $\beta \approx \alpha - 2$, where α is the spectral index, giving a value of $\beta = 0.6 \pm 0.8$. Fits to the dust spectral energy distributions of TMC1 and TMC1A by Chandler et al. (1998) give values of β=1.3$\pm$0.3 for TMC1 and 1.5$\pm$0.6 for TMC1A. We therefore adopt an intermediate value of $\beta = 1$ in calculating the mass of circumstellar material from the dust emission, and use the mass-weighted mean dust temperatures of 22K for TMC1 and 28K for TMC1A derived by Chandler et al., giving $M_{\rm circ} \sim 0.01$ M$_\odot$ for TMC1 and 0.04 M$_\odot$ for TMC1A. The uncertainty in these mass estimates is probably a factor of 5 or so.

3.2 Line Emission

In contrast to the continuum emission from TMC1 and TMC1A the molecular line emission is resolved by the interferometer (Figs. 2 and 3). The line emission traces a greater extent of material than is detected emitting in the continuum. This is due to the excitation requirements for the gas, since in LTE the optical depth of the line emission $\tau \propto N_{\rm CO}/T_{\rm ex}^2$ where $N_{\rm CO}$ is the CO column density and $T_{\rm ex}$ is the excitation temperature, leading to the integrated line emission being proportional to $N_{\rm CO}/T_{\rm ex}$. Thus further from the exciting source, although column densities are lower, the low rotational levels are more highly populated. For dust emission, where $\tau \propto N_{\rm d}$, the emission peaks at the position of maximum $N_{\rm d}T_{\rm d}$, i.e., at the central source.

The ^{13}CO(1–0) and C^{18}O(1–0) emission from TMC1, averaged over 4 channels (0.5 km s^{-1}), is shown in Fig. 2. The ^{13}CO(1–0) emission peaks east of the source in the channels blue-shifted from the systemic velocity of 5.5 km s^{-1}, but there is little detection of red-shifted emission. The same trend is apparent in C^{18}O(1–0), the emission peak moving from east to west as one goes from blue-shifted to red-shifted emission. The maps also seem to be contaminated by outflow, with the emission to the north and south of the continuum source showing much similarity to ^{12}CO maps made of the outflow from this source at similar resolution (Chandler et al. 1996).

The ^{13}CO(1–0) and C^{18}O(1–0) emission from TMC1A, also binned to 0.5 km s^{-1} resolution, is shown in Fig. 3. The ^{13}CO emission peak clearly moves from east to west of the continuum position (marked with a cross) as one goes from blue-shifted to red-shifted emission, relative to the systemic velocity of 6.4 km s^{-1}. This trend is mirrored in the C^{18}O(1–0) data. The emission peak is to the east in the blue-shifted channels from 5.5–6.0 km s^{-1}, is coincident with the continuum peak in the channels between 6.1–6.7 km s^{-1}, and peaks to the west in the channels from 6.8–7.3 km s^{-1}.

Maps of the integrated line emission are presented in Figs 4 and 5. The integrated line fluxes can be used to calculate the total mass of circumstellar gas (cf. Sargent & Beckwith 1987). Using an assumed abundance ratio of ^{13}CO to C^{18}O of 5.5, we find in TMC1A both species are optically thin, with τ(C^{18}O) $\sim$ 0.04. The optical depths are higher towards TMC1 and it is likely that the ^{13}CO is optically thick. We use the integrated C^{18}O emission from both TMC1 and TMC1A to obtain the best estimate for the mass of circumstellar gas in eqn. 3 below, and we have also included a factor of 1.4 to account for the contribution from He:

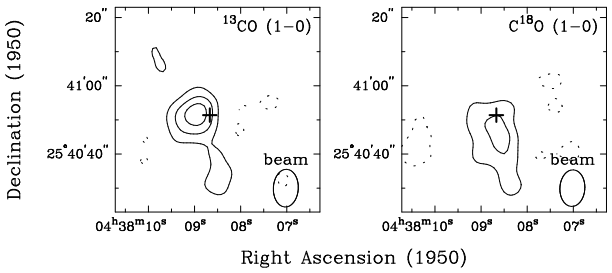

Figure 4. Integrated ^{13}CO(1–0) (left) and C^{18}O(1–0) emission (right) from TMC1. Contour spacing is at the 3σ level of 0.45 Jy km s^{-1} beam^{-1} in the ^{13}CO(1–0) map, and 0.42 Jy km s^{-1} beam^{-1} for the C^{18}O(1–0) emission.

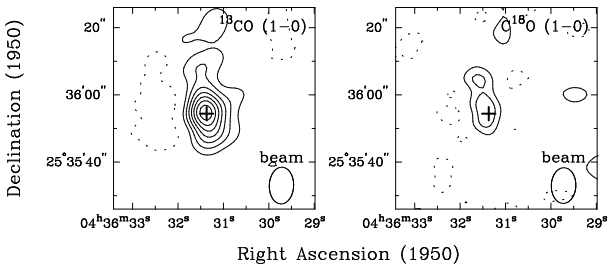

Figure 5. Integrated ^{13}CO(1–0) (left) and C^{18}O(1–0) emission (right) from TMC1A. Contours are spaced at the 3σ level of 0.48 Jy km s^{-1} beam^{-1} for the ^{13}CO(1–0) map, and 0.39 Jy km s^{-1} beam^{-1} for the C^{18}O(1–0) map.

$$M_{\rm tot} = 3.84 \times 10^{-9} \frac{T_{\rm ex} + 0.88}{\exp(-5.27/T_{\rm ex})} \times \frac{D^2}{X({\rm C^{18}O})} \frac{\tau}{(1-e^{-\tau})} \int S_\nu dV \quad {\rm M}_\odot. \quad (3)$$

Here D is the distance to the source in kpc, X(C^{18}O) is the fractional abundance of C^{18}O relative to H$_2$, and $\int S_\nu dV$ the integrated line flux in Jy km s^{-1}. For the Taurus molecular cloud D is taken to be 0.14 kpc (Elias 1978; Kenyon, Dobrzycka, & Hartmann 1994) and we assume X(C^{18}O) =1.7$\times$10^{-7} (Goldsmith, Bergin & Lis 1997). Adopting a value for $T_{\rm ex}$ in the range 10–50 K gives values for the total mass of circumstellar material of $0.02 \leq M_{\rm tot}/{\rm M}_\odot \leq 0.07$ for TMC1 and $0.01 \leq M_{\rm tot}/{\rm M}_\odot \leq 0.03$ for TMC1A. The estimates of the mass of circumstellar material from the integrated C^{18}O emission and the continuum are in good agreement and we conclude that both TMC1 and TMC1A are surrounded by only a few per cent of a solar mass of circumstellar material.

4 MODELLING AND DISCUSSION

The velocity structure in the CO emission from TMC1 and TMC1A may arise from several different dynamical processes commonly observed in the close vicinity of forming protostars. Both sources are already known to be associated with outflow; if the sources are very young it is likely that their envelopes may be infalling, and circumstellar material with high angular momentum will go into

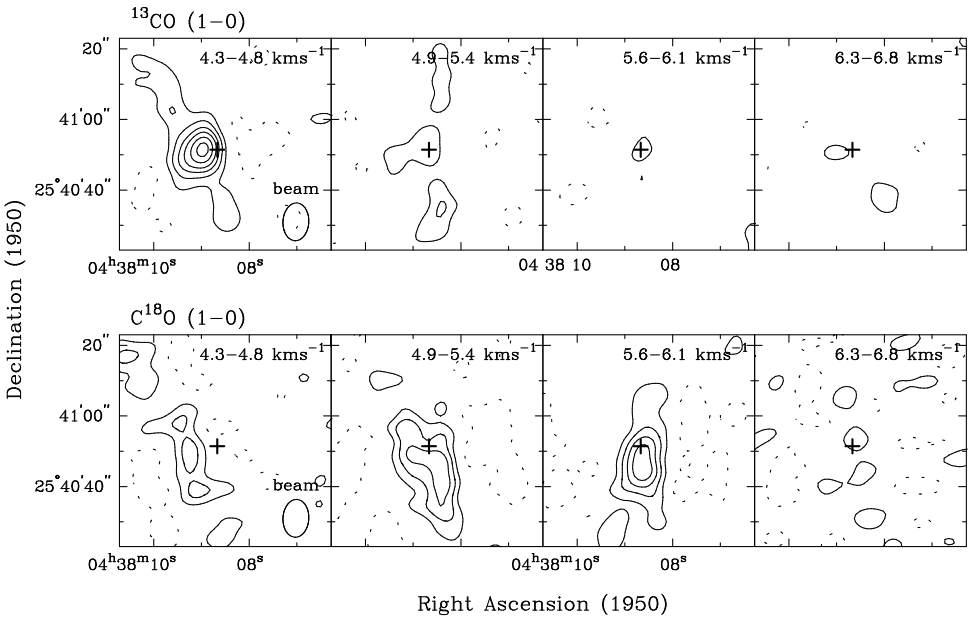

Figure 2. Channel maps of the ^{13}CO(1–0) (top) and C^{18}O(1–0) emission (bottom) from TMC1. The contours in the ^{13}CO(1–0) maps are at 3σ intervals of 0.21 Jy km s^{-1} beam^{-1}, and for the C^{18}O(1–0) maps are at 2σ intervals of 0.14 Jy km s^{-1} beam^{-1}. The emission blue-shifted from the systemic velocity of 5.5 km s^{-1} peaks to the east of the source but the red-shifted emission has been resolved out by the interferometer.

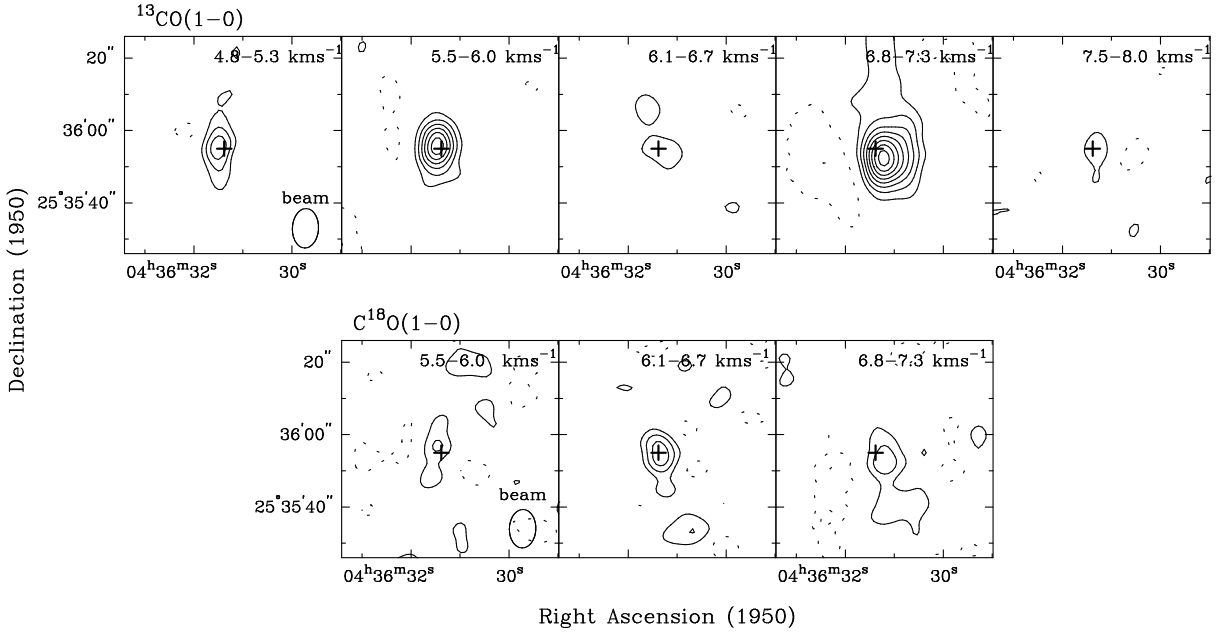

Figure 3. Channel maps of the ^{13}CO(1–0) (top) and C^{18}O(1–0) emission (bottom) from TMC1A. The ^{13}CO maps have contours spaced at the 3σ level of 0.24 Jy km s^{-1} beam^{-1} while the contour spacing is at the 2σ level of 0.13 Jy km s^{-1} beam^{-1} in the C^{18}O maps. As one moves from emission blue-shifted from the systemic velocity of 6.4 km s^{-1} to red-shifted emission the peak emission can be seen to move from east to west with respect to the continuum source (marked with a cross).

rotation about the central star. Thus in order to use the kinematics to determine physical parameters of the system such as the mass of the central object the contributions from each of these processes must be evaluated separately.

Infall has been detected in a number of young systems, e.g., B335, L1527, and L1157 (Chandler & Sargent 1993; Zhou, Evans & Wang 1996; Gueth et al. 1997). In the Shu picture this phase is predicted to last a few $\times 10^5$ years during which the low angular momentum material is accreted, leaving the higher angular momentum gas in a rotating disc or envelope. The characteristic signature of infall is an asymmetric emission line from optically thick tracers, with red-shifted self-absorption and a blue-shifted

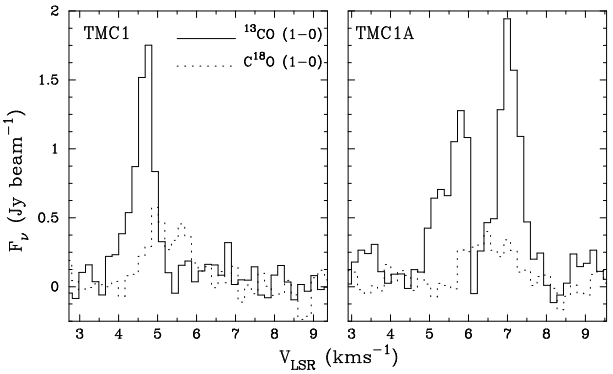

Figure 6. ^{13}CO and C^{18}O line profiles obtained by averaging the emission in a $10'' \times 10''$ region centred on each source. The systemic velocities of the sources are 5.5 km s^{-1} and 6.4 km s^{-1} for TMC1 and TMC1A respectively.

peak stronger than the red-shifted peak, whilst optically thin lines remain symmetric about the cloud systemic velocity (e.g., Snell & Loren 1977; Zhou 1992).

The ^{13}CO and C^{18}O (1–0) line profiles of TMC1 and TMC1A, averaged over a region $10'' \times 10''$ centred on each continuum source, are shown in Fig. 6. The profiles of TMC1A show no evidence for significant mass infall: the red-shifted ^{13}CO(1–0) peak is stronger than the blue-shifted peak, contrary to that expected for infalling gas. It is less clear from the line profiles whether the same can be said of TMC1, as the red-shifted emission is almost completely lacking from the ^{13}CO(1–0) dataset, and if the C^{18}O(1–0) emission is optically thin it is not expected to reveal an asymmetric profile. The interferometric and single-dish line profiles presented by Hogerheijde et al. (1998) also show little evidence for infall for either TMC1 or TMC1A, and are assumed in their work to arise from rotating envelopes with contributions from outflow. This interpretation is supported by first moment (intensity-weighted mean $V_{\rm LSR}$) maps of the envelope emission (Fig. 7). The first moment map of TMC1A shows a distinct velocity gradient in the ^{13}CO(1–0) emission oriented close to 90° to the direction of outflow, consistent with rotation in an envelope. The C^{18}O(1–0) first moment map of TMC1 has a velocity gradient aligned at approximately 45° to the outflow axis, which is what one would expect if it contained contributions from both outflow and rotation.

Position-velocity (P–V) diagrams, obtained by taking cuts through the data cubes perpendicular to the outflow axes, can also be used to argue against the presence of infall in TMC1 and TMC1A (Fig. 8*a*). The expected signature of infall in a P–V diagram is red- and blue-shifted peaks which coincide with the source position. Pure rotation has the red-shifted emission confined to one side of the source and blue-shifted emission to the other; combinations of infall and rotation are intermediate between these two extremes (Ohashi et al. 1997a). Outflows, for which the molecular gas typically accelerates away from the star, can be distinguished from rotation and infall by the characteristic increase in velocity with distance from the source (e.g., Bachiller 1996).

4.1 Modelling the ^{13}CO and C^{18}O J=1–0 Line Emission

The velocity structure observed in Figs 7 and 8*a* leads us to conclude that the dominant motion in the circumstellar envelopes of TMC1 and TMC1A is rotation. By taking a cut through the envelopes perpendicular to the rotation axis we minimise the possible

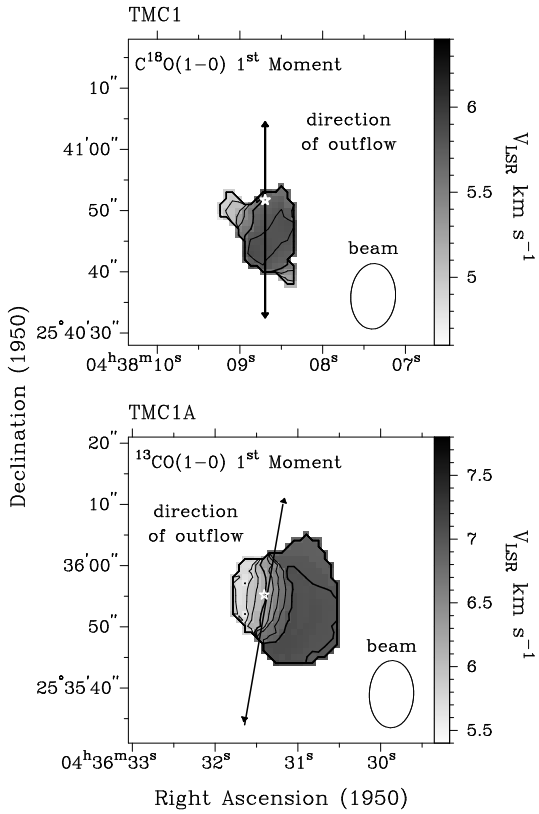

Figure 7. First moment (intensity-weighted mean $V_{\rm LSR}$) maps of the C^{18}O(1–0) emission from TMC1 and ^{13}CO(1–0) emission from TMC1A. A distinct velocity gradient aligned close to 90° to the direction of outflow can be seen in the TMC1A data. The velocity gradient in the C^{18}O emission from TMC1 is aligned somewhere between the direction expected due to emission from an outflow and that expected from a rotationally flattened envelope, suggesting a contribution from both components. The TMC1 map has isovelocity contours spaced at 0.2 km s^{-1} from 4.6 km s^{-1} to 6.4 km s^{-1}. The contours in the TMC1A map are spaced at 0.2 km s^{-1} and run from 5.4 km s^{-1} to 7.8 km s^{-1}.

contamination by outflow which would result from attempting to fit the channel maps directly. We expect the envelopes to be rotationally flattened, an assumption which is supported by the interferometric imaging of the HCO$^+$(1–0) emission from both sources at $5''$ resolution by Hogerheijde et al. (1998). As our primary aim is to determine the stellar masses of TMC1 and TMC1A we adopt a simple disc model to describe the velocity structure in the circumstellar gas. The difference in a disc model and one of a flattened envelope lies mainly in the form of the surface density, Σ. As the results from the modelling show (see Table 1), the data are insensitive to the precise form of the surface density but the kinematics define the central mass extremely well. This is confirmed by the recent results of Momose et al. (1998), who model C^{18}O emission from L1551 IRS 5 and show that the stellar mass derived from P–V diagrams by assuming a geometrically thin disc morphology is in good agreement with more elaborate models of flattened envelopes and envelopes with bipolar cavities.

The line emission from the disc is calculated assuming LTE, and is then convolved with our beam. A model P–V diagram is produced by taking a cut along the major axis of the disc, and a χ^2 minimisation is performed to the observed P–V diagrams (Fig. 8*a*) to obtain the mass of the central star and the temperature and dens-

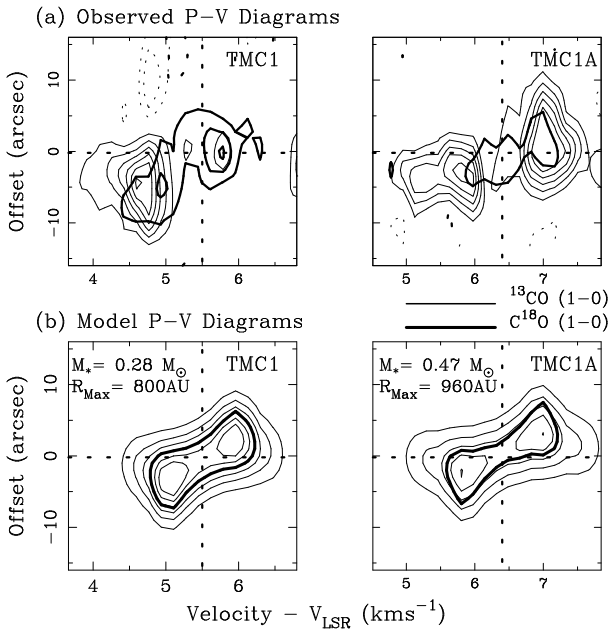

Figure 8. (*a*) Position–velocity diagrams for TMC1 and TMC1A in ^{13}CO(1–0) (light) and C^{18}O(1–0) (bold). The dotted line in each frame indicates the continuum position of the source and the systemic velocity. Contours are set at the 2σ level for both sources, 0.41 Jy beam^{-1} for TMC1 and 0.42 Jy beam^{-1} for TMC1A in ^{13}CO, and 0.37 Jy beam^{-1} for TMC1 and 0.35 Jy beam^{-1} for TMC1A in C^{18}O. (*b*) Model fits to the observed P–V diagrams for inclination $i = 55^\circ$, and the other parameters given in the figure.

ity distributions in the disc. To simplify the model the velocity field is assumed to be determined solely by the mass of the central, point-like, stellar object. This approach is justified by the small masses of circumstellar gas derived in section 3 above, which is an order of magnitude smaller than previous estimates of the central masses based on dynamical arguments (Ohashi et al. 1997b, Hogerheijde et al. 1997) or on the source luminosities (Hogerheijde et al. 1997). Radial power law expressions are adopted for the temperature distribution, $T = T_0 r^{-q}$, and the surface density, $\Sigma = \Sigma_0 r^{-p}$. At large radii the mean temperature of the Taurus cloud places a lower limit of $T = 10$ K. We then perform a χ^2 minimisation to fit for the central stellar mass, M_*, the disc radius, $R_{\rm max}$, T_0, q, Σ_0, and p using the Levenberg-Marquardt method (Press et al. 1987).

The blue-shifted ^{13}CO(1–0) emission from TMC1A (Fig. 8*a*) between $V_{\rm LSR} = 4.8$ and 5.5km s^{-1} may be due to outflow, and shows the characteristic acceleration with distance from the central source (e.g. Bachiller 1996). The absence of emission near the systemic velocity is also significant for the ^{13}CO, and results from the high optical depth in the line centre causing the extended $\tau = 1$ surface to be resolved out by the interferometer. Care must therefore be taken to include only those channels which can reliably be assigned to the rotating envelope when fitting the P–V diagrams. If channels containing outflow were included in the fit to the data, and the velocities interpreted as purely rotational, the effect would be to increase the derived stellar mass. For this reason we take the C^{18}O channels where we have detected emission, i.e., $V_{\rm LSR} = 6.0$ to 7.3km s^{-1}, and fit the shape of the P–V diagram and intensity of emission. We do the same for the ^{13}CO but omit the channels near to the systemic velocity of 6.4 km s^{-1} where the emission has been resolved out by the interferometer. The abundance ratio of ^{13}CO to C^{18}O is assumed to be 5.5.

For TMC1 the optical depth of ^{13}CO(1–0) is higher than in TMC1A suggesting that it is more deeply embedded, with a possible layer of occluding foreground material inferred from the HCO$^+$(1–0) observations of Hogerheijde et al. (1998). The only emission detected in ^{13}CO from TMC1 is blue-shifted from the systemic velocity. From comparisons between the channel maps, and observations of the outflow made in ^{12}CO(1–0) (Chandler et al. 1996), it seems likely that the ^{13}CO emission arises in the most part from the outflow. The ^{13}CO data are therefore not included in the fit to the P–V diagram for TMC1. Indeed, were these motions interpreted as being rotational the required central mass would be $\gtrsim 1$ M$_\odot$, which seems unlikely given its low bolometric luminosity of 0.62 L$_\odot$ (Chandler et al. 1998). For TMC1 we make the fit to the C^{18}O emission which does show peaks at velocities closer to the systemic velocity of the source. These data still contain some extended, high velocity blue-shifted emission, which suggests that these data may contain contributions from both the outflow and the rotating envelope.

Typical fits to the P–V diagrams are shown in Fig. 8*b*, and the best-fit values for the model parameters, along with the errors obtained from the covariance matrix, are given in Table 1. The largest uncertainty in determining the stellar mass is the unknown inclination of TMC1 and TMC1A to the line of sight. This has been estimated for both sources to be between 40°–70° by Chandler et al. (1996) where 0° corresponds to a face on disc. Fits to the data within this range of inclination angles were investigated and the values obtained for the extreme values of the inclination are listed in Table 1. Fits to the P–V diagrams illustrate that the model is most sensitive to the mass of the central source, which determines the velocity structure of the gas, and to the disc radius, which fixes the extent of the emission. Note, however, that the best-fit values of $R_{\rm max}$ are close to the largest angular scale which can be imaged by the interferometer, and may be an artifact of the imaging technique used rather than representing a physical disc size. An increase in surface density increases the optical depth and thus reduces the ratio of ^{13}CO to C^{18}O emission, whilst an increase in temperature has the opposite effect. The fitted values of the temperature and surface density are therefore correlated, resulting in larger uncertainties. It is possible to constrain these parameters by rejecting physically unlikely solutions, i.e., those with unreasonably high temperatures at large radii, or with a surface density decreasing too steeply with r.

4.2 Previous Mass Estimates for TMC1 and TMC1A

Our disc model predicts stellar masses of 0.2–0.4 M$_\odot$ for TMC1 and 0.35–0.7 M$_\odot$ for TMC1A, comparable to the masses of visible T Tauri stars in Taurus (Kenyon et al. 1990). The value we calculate for TMC1 is not consistent with that derived by Hogerheijde et al. (1998), who quote a mass of ~ 0.8 M$_\odot$ assuming an inclination of 55°, a systemic V$_{\rm LSR}$ of 5.2 km s^{-1}, and use a P–V diagram of HCO$^+$(1–0) emission obtained at P.A.=0°. If the true cloud velocity is at V$_{\rm LSR} = 5.5$ km s^{-1} as measured by Terebey, Vogel, & Myers (1989), the value adopted in this paper, then the stellar mass obtained from the HCO$^+$ data would be even higher, which presents severe difficulties explaining its low luminosity ($L_{\rm bol} = 0.62$ L$_\odot$). A possible explanation for this discrepancy is that the HCO$^+$ observations are tracing outflow, and do not reflect the motion of material in a rotating envelope.

The mass we obtain for TMC1A compares well with the value derived from the kinematics by Ohashi et al. (1997b), who obtain a

mass of 0.5 $M_\odot$ for an inclination of 50°. Hogerheijde et al. (1998) also derive a mass for TMC1A from HCO^+(1–0) emission, in this case only detecting emission red-shifted relative to the systemic velocity of the source. They quote a mass for TMC1A of 0.2 $M_\odot$ for an inclination of 55°, but again use a different systemic V_{LSR} of 6.6 km s^{-1} compared with the 6.4 km s^{-1} adopted here (Terebey et al. 1989). This would cause Hogerheijde et al. to underestimate the mass of TMC1A. Furthermore, their P–V diagram is a cut at P.A.= 65° while the outflow is aligned at P.A.=−10° (Chandler et al. 1996), also suggesting they may not be sampling the maximum velocity gradient, which would also result in a low mass estimate.

4.3 Implications for the Mass Accretion Rate

Kenyon et al. (1990) compare the number of embedded protostars detected by IRAS to the number of T Tauri stars in Taurus and estimate the embedded phase of star formation to last $\sim 10^5$ years. If the embedded stars are assumed to be similar in mass to the T Tauri population then a mean accretion rate of $\sim 2-4\times10^{-6}M_\odot yr^{-1}$ is needed to assemble a star in the lifetime of the embedded phase. However, the median luminosity of the embedded sources of $\sim 1L_\odot$ implies an accretion rate an order of magnitude smaller, and leads to the 'Class I luminosity problem' (Kenyon et al. 1990). We have used the kinematics of the circumstellar gas around TMC1 and TMC1A to confirm that M_*(Class I) $\simeq M*$ (T Tauri), and place an upper limit on their accretion rates by assuming that accretion is the sole source of the luminosity. Using equation 1 and assuming a typical protostellar radius of $R_* \sim 3$ $R_\odot$ (Stahler 1988) we find $\dot{M} \lesssim 2-4\times10^{-7}M_\odot$ yr^{-1} for TMC1 and TMC1A. The well determined masses of TMC1 and TMC1A tightly constrain the rate of accretion to the star implying an order of magnitude difference between the theoretical and observed accretion rates.

A possible source of uncertainty in the accretion rate may arise when determining the bolometric luminosities. Men'shchikov & Henning (1997) have shown for L1551–IRS5 that the derived luminosity may be affected by viewing angle by as much as a factor of two if isotropic radiation in spherical geometry is assumed. In L1551–IRS5 the line of sight to the central protostar is relatively unobscured by the circumstellar envelope. This leads to a view of the disc surface directly heated by the central star. If a combination of narrow outflow opening angles and sources lying close to the plane of the sky occurs, as has been shown to be the case for TMC1 and TMC1A (Chandler et al. 1996), the line of sight passes through a large column density of cold obscuring material, lowering the estimate of the bolometric luminosity. While underestimating the bolometric luminosities may contribute to the shortfall in the luminosities of the protostars in Taurus, it is unlikely to explain the order of magnitude differences in the observed and theoretical accretion rates.

A more likely explanation for the low luminosities of protostars in Taurus is accretion that is not constant in time. One possibility is that at early times the mass accretion was high and has decreased monotonically to the values observed now. Henriksen, André & Bontemps (1997) use a study of outflow activity in low-mass embedded protostars and the observed radial density profiles of pre-collapse starless cores to construct such a model. Assuming a connection between accretion rate and outflow power, the high outflow luminosities of young, Class 0, protostars relative to Class I sources imply initially high accretion rates, possibly decaying to a rate similar to the Shu model, with a phase of declining accretion thereafter for the final remnants of circumstellar material. The fact that observations of pre-stellar cores show density profiles flatter than the r^{-2} profile predicted for singular isothermal spheres in their inner regions provides the mechanism for the time variability of the accretion rate.

An alternative model for non-constant infall proposes FU Orionis type accretion for embedded protostars (Hartmann & Kenyon 1985, 1987). In this picture accretion initially occurs to a disc at large radii. The system spends the majority of its time in a quiescent state where accretion onto the central protostar star is at a low level of $\dot{M} \sim 10^{-7}$ $M_\odot yr^{-1}$, while accretion onto the disc proceeds at a faster rate until the disc becomes gravitationally unstable. A period of rapid accretion then follows at a rate of $\sim 10^{-4}$ $M_\odot yr^{-1}$ lowering the disc mass to a point where it becomes stable again and the low accretion rate from the disc onto the star is resumed. The luminosity history of the source is characterised by long periods of low luminosity and low accretion, punctuated by short-lived periods of high luminosity and rapid accretion with the majority of the mass being accumulated during these rapid accretion phases. FU Ori disc models predict that a low mass star typically spends $\sim 5\%$ of its time in the high accretion phase (Hartmann & Kenyon 1996) thus one might expect to observe approximately one source in twenty to be in outburst at any one time. Given that the Taurus molecular cloud has ~ 20 embedded sources, and one source, L1551 IRS 5, has been classed as a potential FU Ori type variable (Mundt et al. 1985), these estimates do agree, but the sample is too small for a proper statistical test of the model.

There is clearly a marked difference in the accretion histories predicted by the Henriksen et al. and the Hartmann & Kenyon models, so it should be possible to distinguish between them with mass measurements of a complete population of embedded protostars with a large range of ages. The stage at which the models differ most significantly is early on in the collapse process, where the Henriksen et al. model predicts far greater mass infall rates. Measurement of the masses and accretion rates for the youngest protostars will therefore be essential for establishing how $\dot{M}$ varies with time.

5 CONCLUSIONS

Continuum measurements at 2.7mm, and observations of ^{13}CO and $C^{18}O$ J=1–0 line emission have been made towards two protostars in Taurus, TMC1 and TMC1A. These observations reveal the presence of molecular gas out to radii of ~ 1000 AU, and trace rotating envelopes with masses $\sim 0.03M_\odot$. Position–velocity diagrams of these sources obtained perpendicular to their outflow axes are well fitted by a Keplerian velocity field. Modelling the kinematic structure of the envelopes gives central stellar masses of 0.2–0.4 $M_\odot$ for TMC1 and 0.35–0.7 $M_\odot$ for TMC1A for inclinations between the measured limits of 40°–70° (Chandler et al. 1996). Adopting a fixed value for the inclination enables us to calculate the stellar mass to an accuracy of $\sim 10\%$.

The use of kinematics to determine the central mass is the only reliable method currently available. Having well constrained mass estimates enables us to calculate upper limits to the accretion rates for these sources by assuming the bolometric luminosities of these protostars is derived solely from accretion. The measured accretion rate is an order of magnitude lower than the theoretical infall rate from the standard model of the collapse of a singular isothermal sphere (Shu 1977). The accretion rates measured for TMC1 and TMC1A are too low to accumulate their stellar masses during the estimated lifetime of the embedded phase of star formation in Taurus (Kenyon et al. 1990). This leads to the conclusion

that to assemble solar mass size objects before the termination of the embedded phase requires accretion rates that are not constant in time. Whilst these observations cannot distinguish between the time-dependent accretion models of Henriksen et al. (1997) and Hartmann & Kenyon (1985, 1987), measurements of $\dot{M}$ as a function of M_* for a complete population of embedded sources, particularly the youngest, most deeply embedded protostars, should be extremely important for constraining alternative accretion histories.

ACKNOWLEDGEMENTS

We would like to thank the referee for suggestions which improved the clarity of the text. CJC was supported by an Advanced Fellowship from the Particle Physics and Astronomy Research Council during most of this work, and DWB acknowledges the receipt of a PPARC Research Studentship. Astronomy at the Owens Valley Radio Observatory is supported by the National Science Foundation, contract AST 96–13717.

REFERENCES

Bachiller, R., 1996, ARA&A, 34, 111
Beckwith, S.V.W., Sargent, A.I., 1991, ApJ, 381, 250
Beckwith, S.V.W., Sargent, A.I., Chini, R.S., Güsten, R., 1990, ApJ, 99, 924
Briggs, D., 1995, BAAS, 187, 112
Chandler, C.J., Sargent, A.I., 1993, ApJ, 414, L29
Chandler, C.J., Terebey, S., Barsony, M., Moore, T.J.T., Gautier, T.N., 1996, ApJ 471, 308
Chandler, C.J., Barsony, M., Moore, T.J.T., 1998, MNRAS, in press
Chen, H., Myers, P.C., Ladd, E.F., Wood, D.O.S., 1995, ApJ, 445, 377
Draine, B.T., Lee, H.M., 1984, ApJ, 285, 89
Elias, J.H., 1978, ApJ, 224, 857
Foster, P.N., Chevalier, R.A., 1993, ApJ, 416, 303
Goldsmith, P.F., Bergin, E.A., Lis, D.C., 1997, ApJ, 491, 615
Goodman, A.A., Benson, P.J., Fuller, G.A., Myers, P.C., 1993, ApJ, 406, 528
Gueth, F., Guilloteau, S., Dutrey, A., Bachiller, R., 1997 A&A, 323, 943
Hartmann, L., Kenyon, S.J., 1985, ApJ, 299, 462
Hartmann, L., Kenyon, S.J., 1987, ApJ, 312, 243
Hartmann, L., Kenyon, S.J., 1996, ARA&A, 34, 207
Henriksen, R., André, P., Bontemps, S., 1997 A&A, 323, 549
Hildebrand, R.H., 1983, QJRAS, 24, 267
Hogerheijde, M.R., van Dishoeck, E.F., Blake, G.A., van Langevelde, H.J., 1997, ApJ, 489, 293
Hogerheijde, M.R., van Dishoeck, E.F., Blake, G.A., van Langevelde, H.J., 1998, ApJ, in press
Kenyon, S.J., Hartmann, L.W., Strom, K.M., Strom, S. E., 1990, AJ, 99, 869
Kenyon, S.J., Dobrzycka, D., Hartmann, L., 1994, AJ, 108, 1872
Krügel, E., Siebenmorgen, R., 1994, A&A, 288, 929
Lay, O.P., Carlstrom, J.E., Hills, R.E., Phillips, T.G., 1994, ApJ, 434, L75
Lay, O.P., Carlstrom, J.E., Hills, R.E., 1997, ApJ, 489, 917
Looney, L.W., Mundy, L.G., Welch, W.J., 1997, ApJ, 484, L157
Mannings, V., Emerson, J.P., 1994, MNRAS, 267, 361
Men'shchikov, A.B., Henning, T., 1997, A&A, 318, 879
Momose, M., Ohashi, N., Kawabe, R., Nakano, T., Hayashi, M., 1998, ApJ, in press
Mundt, R., Stocke, J., Strom, S.E., Strom, K.M., Anderson, E.R., 1985, ApJ, 297, L41
Ohashi, N., Hayashi, M., Kawabe, R., Ishiguro, M., 1996, ApJ, 466, 317
Ohashi, N., Hayashi, M., Ho, P.T.P., Momose, M., 1997a, ApJ, 475, 211
Ohashi, N., Hayashi, M., Ho, P.T.P., Momose, M., Tamura, M., Hirano, N., Sargent, A.I., 1997b, ApJ, 488, 317
Pollack, J.B., Hollenbach, D., Beckwith, S., Simonelli, D.P., Roush, T., Fong, W., 1994, ApJ, 421, 615
Press, W.H, Flannery, B.P., Teukolsky, S.A., Vetterling, W.T., 1987, 'Numerical Recipes: The Art of Scientific Computing' Cambridge University Press, Cambridge
Sargent, A.I., Beckwith, S., 1987, ApJ, 323, 294
Scoville, N.Z., Carlstrom, J.E., Chandler, C.J., Phillips, J.A., Scott, S.L., Tilanus, R.P.J., Wang, Z., 1993, PASP, 105, 1482
Shu, F.H., 1977, ApJ, 214, 488
Snell, R.L., Loren, R.B., 1977, ApJ, 211, 122
Stahler, S.W., 1988, ApJ, 332, 804
Terebey, S., Shu, F.H., Cassen P., 1984, ApJ, 286, 529
Terebey, S., Vogel, S.N., Myers, P.C. 1989, ApJ, 340, 472
Terebey, S., Chandler, C.J., André, P., 1993, ApJ, 414, 759
van Langevelde, H.J., van Dishoeck, E.F., Blake, G.A., 1994, ApJ, 425, L45
Wilner, D.J., Ho, P.T.P., Rodriguez, L.F., 1996, ApJ, 470, L117
Wright, E.L., 1987, ApJ, 320, 818
Zhou, S., 1992, ApJ, 394, 204
Zhou, S., Evans, N.J., II, Wang, Y., 1996, ApJ, 466, 296

This paper has been produced using the Royal Astronomical Society/Blackwell Science LaTeX style file.

Table 1. Best-fit disc model parameters for TMC1 and TMC1A

Source	inclination	M_*	R_{max}	Σ_0	p	$T_{100\,AU}$[a]	q
	(°)	($M_\odot$)	(AU)	($\times 10^{16}$ m^{-2})		(K)	
TMC1	40	0.38±0.03	800±30	6.9±5.7	1.2±0.6	65±61	0.4±0.6
	70	0.20±0.02	950±50	7.2±6.7	1.4±0.7	70±67	0.1±0.7
TMC1A	40	0.73±0.04	950±30	2.1±0.5	2.0±0.3	135±111	1.4±0.6
	70	0.35±0.02	970±50	3.2±1.0	1.8±0.3	155±99	1.1±0.3

[a] Disc temperature at a radius of 100 AU.